CJC Chinese Journal of Chemistry 中国化学 - An International Journal

Concise Report

Cite this paper: *Chin. J. Chem.* **2026**, *44*, 73—79. **DOI: 10.1002/cjoc.70313**

Compatibility Integrated Sulfide-Based Cathode and Electrolyte for High-Energy Solid-State Sodium Batteries†

Hewei Xu,*[,a,b] Xiaodong Lin,*[,b] Hong Chang,[a] Petru Apostol,[b] Jiande Wang,[b] Xuelian Liu,[b] Xiaozhe Zhang,[b] Da Tie,[b] and Alexandru Vlad*[,b]

[a] *Taiyuan Institute of Technology, Department of Materials Engineering, Taiyuan, Shanxi 030008, China*
[b] *Institute of Condensed Matter and Nanosciences, Université Catholique de Louvain, Louvain-la-Neuve, B-1348, Belgium*

Keywords

Sodium batteries | Sulfide solid electrolyte | Na_2MoS_4 | Sulfide-based cathode | Solid-state batteries | Energy storage | Amorphous materials | Electrochemistry

Comprehensive Summary

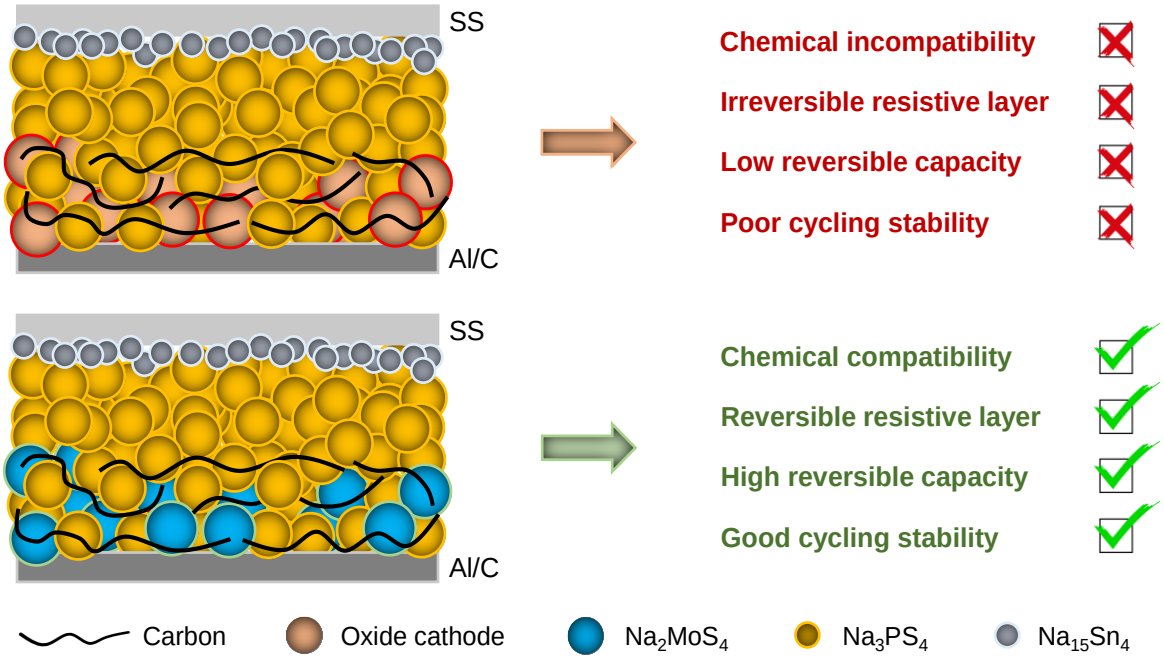

The scarcity of critical raw materials in lithium-ion batteries has driven increasing interest in alternative chemistries, such as sodium-based all-solid-state batteries. Among various solid electrolytes, sulfide-based Na_3PS_4 stands out for its high ionic conductivity and excellent formability. However, its poor interfacial compatibility with conventional high-voltage oxide cathodes remains a major limitation. In this study, we report the successful integration of amorphous Na_2MoS_4—a high-capacity, sulfide-compatible cathode—into Na_3PS_4-based all-solid-state sodium batteries. Benefiting from a moderate redox potential window (1.1–2.7 V vs. Na^+/Na), Na_2MoS_4 exhibits excellent chemical and electrochemical compatibility with Na_3PS_4, as confirmed by structural and spectroscopic analyses. Further investigation reveals that intimate interfacial contact between both electrodes and the solid-state electrolyte is critical for achieving long-term cycling stability. Based on these insights, the optimized $Na_{15}Sn_4$ | Na_3PS_4 | Na_2MoS_4-Na_3PS_4-carbon nanofiber cell delivers a reversible capacity of ~372 mAh·g^{-1} at 0.1 C and retains nearly 100% capacity over 450 cycles at 0.3 C. *In situ* impedance spectroscopy further confirms the stability of interfacial resistance throughout cycling. This work identifies Na_2MoS_4 as a highly promising sulfide cathode for high-energy, long-life sodium solid-state batteries and provides valuable design principles for future development of sulfide-based electrode-electrolyte interfaces in next-generation energy storage systems.

*E-mail: xuhewei@tit.edu.cn; xiaodong.lin@uclouvain.be; alexandru.vlad@uclouvain.be
† Dedicated to the Special Issue of Emerging Investigators in 2025.

For submission: https://wiley.atyponrex.com/journal/CJOC
For published articles: https://onlinelibrary.wiley.com/journal/16147065

Background and Originality Content

Lithium-ion batteries (LIBs) currently dominate the energy storage sector. However, as demand grows, particularly with the expansion of electric vehicles and stationary storage, resource availability and supply chain stability are expected to come under increasing strain. The long-term viability of LIB technology is challenged by the limited availability of critical raw materials, especially cobalt (Co) and lithium (Li). This poses a significant concern for the energy storage industry, as escalating demand may further intensify the scarcity of these essential elements.[1] Consequently, alternative technologies, such as sodium-ion batteries (SIBs), are being actively explored as more sustainable and cost-effective energy storage solutions.[2]

All-solid-state sodium batteries employing inorganic solid electrolytes have attracted significant global interest for large-scale energy storage applications, owing to their improved safety and lower cost compared to non-aqueous liquid sodium-ion batteries.[3-8] Among the various Na^+-conducting solid electrolytes, sulfide-based systems are particularly promising due to their excellent formability and high ionic conductivity.[9-10] However, their practical deployment is limited by interfacial compatibility issues with high-voltage oxide cathodes.[11] Specifically, the operating voltage of these cathodes exceeds the anodic decomposition potential of Na_3PS_4, leading to the formation of a resistive interfacial layer (Figure 1a), which increases interfacial resistance and deteriorates electrochemical performance.[12-14] In addition, the chemical potential mismatch between oxide cathodes and Na_3PS_4 can result in the formation of a highly resistive space charge layer at the interface.[15]

To address this interfacial issue, Yao *et al.* proposed the use of organic materials with moderate redox potentials, such as pyrene-4,5,9,10-tetrone (PTO), to replace high-voltage oxides as suitable cathodes for sulfide-based solid-state electrolyte systems. This strategy effectively resolves the interfacial compatibility problem and enables excellent electrochemical performance.[11]

In the case of inorganic cathode systems, it is generally accepted that transition metal sulfides exhibit superior compatibility with sulfide-based solid-state electrolytes compared to transition metal oxides (Figure 1a). This is attributed to their moderate redox potential windows and chemical potentials. However, only a limited number of transition metal sulfides such as TiS_2,[16-17] $Fe_{1-x}S_2$,[18] and MoS_2,[19] have been investigated in such systems (Figure 1b), leaving many other promising candidates yet to be explored. For example, amorphous Na_2MoS_4 is a promising sulfide-based metal cathode material for use in sulfide solid-state electrolytes, owing to its moderate electrochemical window (1.1–2.7 V vs. Na^+/Na) and high theoretical specific capacity of up to 500 $mAh{\cdot}g^{-1}$, corresponding to a five-electron redox process.[20]

In this work, we investigated the applicability of Na_2MoS_4 in Na_3PS_4-based solid-state electrolyte systems. The results show that Na_2MoS_4 exhibits excellent chemical and electrochemical compatibility with Na_3PS_4. By enhancing interfacial contact among the components within the composite cathode and improving interfacial stability at the anode side, we achieved outstanding electrochemical performance in the Na_2MoS_4-Na_3PS_4 solid-state battery system. This system delivers a reversible specific capacity of up to 372 $mAh{\cdot}g^{-1}$ and a material-level energy density of ~700 $Wh{\cdot}kg^{-1}$ at 0.1 C. Furthermore, it exhibits excellent rate and cycling performance, maintaining a discharge capacity of 200 $mAh{\cdot}g^{-1}$ at 1 C, with negligible capacity decay over 450 cycles at 0.3 C. These results confirm that Na_2MoS_4 is a highly promising sulfide metal cathode material for use in sulfide-based solid-state batteries.

Results and Discussion

Chemical compatibility between Na_2MoS_4 and Na_3PS_4

The Na_3PS_4 solid-state electrolyte (Figure S1) and Na_2MoS_4 cathode material (Figure S2) used in this study were both synthesized following previously reported methods.[10,16,20] Electrochemical impedance spectroscopy (EIS) measurements revealed ionic conductivities of 1.6×10^{-4} $S{\cdot}cm^{-1}$ at 25 °C and 5.0×10^{-4} $S{\cdot}cm^{-1}$ at 60 °C (Figure S3), meeting the ionic conductivity requirements for electrochemical reactions in solid-state batteries.

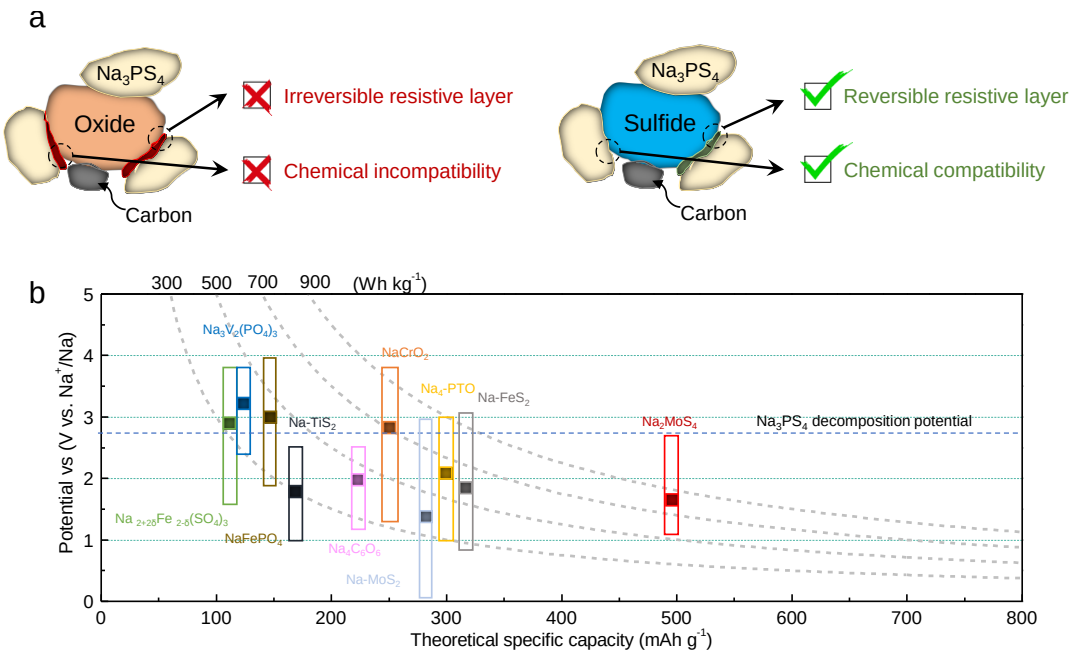

Figure 1 Interfacial compatibility between cathode materials and sulfide solid electrolytes. (a) Schematic comparison of electrode-electrolyte interfaces between oxide cathodes/sulfide cathodes and the Na_3PS_4 solid electrolyte. (b) Plot of redox potential versus theoretical specific capacity for representative intercalation-type cathode materials (TiS_2,[10,26-28] $Na_3V_2(PO_4)_3$,[29-30] $NaFePO_4$,[31-32] $Na_{2+2\delta}Fe_{2-\delta}(SO_4)_3$,[33] $NaCrO_2$,[34-35], $Na_4C_6O_6$[36] and Na4-PTO[11]), Na_2MoS_4 (this work), and selected conversion-type cathodes (MoS_2[16] and FeS_2[37]). Theoretical specific capacities are calculated based on the fully sodiated form of each cathode material. Solid squares and open bars represent the average redox potentials and corresponding electrochemical windows, respectively

To mitigate decomposition of the sulfide-based electrolyte during charge-discharge cycling, carbon nanofiber (CNF) was employed as the conductive additive in the composite cathode, owing to their relatively low specific surface area compared to other carbon materials, which helps suppress interfacial side reactions.[21] Prior studies have indicated that a color change upon mixing active materials with sulfide-based electrolytes can serve as a qualitative indicator of chemical compatibility.[22] Based on the intrinsic colors of Na_2MoS_4 (black) and Na_3PS_4 (light yellow), and the resulting grey-black mixture (Figure S4)—suggestive of a simple physical blending without significant chemical interaction—we preliminarily conclude that Na_2MoS_4 exhibits good chemical compatibility with Na_3PS_4.

To further confirm the chemical compatibility between Na_2MoS_4 and Na_3PS_4, spectroscopic characterizations including X-ray diffraction (XRD) and Fourier-transform infrared spectroscopy (FTIR) were conducted. As Na_2MoS_4 is an amorphous material,[20] the XRD pattern of the Na_2MoS_4-Na_3PS_4-CNF mixture (Figure 2a) exhibited only the characteristic peaks of Na_3PS_4 and CNF, with no additional diffraction peaks observed, indicating a simple physical mixture without the formation of new crystalline phases. Similarly, FTIR spectra of the Na_2MoS_4-Na_3PS_4 mixture (without CNF) showed a superposition and slight shift of the characteristic absorption bands—P–S (from Na_3PS_4), and Mo–S and S–S (from Na_2MoS_4)—without the appearance of new bands.[23-25] These results clearly demonstrate that Na_2MoS_4 and Na_3PS_4 exhibit excellent chemical compatibility, with no chemical reaction occurring upon mixing, thereby ensuring interfacial stability in composite cathode during battery operation.

Cell performance

To further evaluate the electrochemical compatibility between Na_2MoS_4 and Na_3PS_4, we conducted a series of electrochemical tests on an all-solid-state battery integrating both components. To closely approximate the low stacking pressure conditions and cost constraints relevant to practical applications, sodium metal was directly used as the anode, and a coin cell configuration was employed for performance evaluation. As shown in Figure S5, the Na | Na_3PS_4 | Na_2MoS_4-Na_3PS_4-CNF solid-state battery with the optimized composite cathode composition delivers a reversible specific capacity of up to 450 mAh·g^{-1} at a current rate of 0.1 C within a voltage window of 0.65–3.2 V (vs. Na^+/Na), corresponding to a material-level energy density of ~700 Wh·kg^{-1}. Figures 3a and 3b illustrate the rate performance of this battery system. At current rates of 0.1 C, 0.2 C, 0.3 C, 0.5 C, and 1.0 C, the cell delivers specific capacities of approximately 381, 286, 188, 52, and 3 mAh·g^{-1}, respectively. Notably, when the current rate was reduced back to 0.2 C, the capacity nearly recovered to its original level, indicating that Na_2MoS_4 retains good structural stability during high-rate cycling. To exclude any capacity contribution from the Na_3PS_4-based sulfide solid-state electrolyte, control experiments were performed using a composite cathode without Na_2MoS_4. As shown in Figure 3c, the Na | Na_3PS_4 | Na_3PS_4-CNF cell exhibited negligible capacity, confirming that the observed capacity in the Na | Na_3PS_4 | Na_2MoS_4-Na_3PS_4-CNF battery originates primarily from the redox activity of Na_2MoS_4 rather than the electrolyte.

However, it is important to note that the poor chemical and electrochemical compatibility between metallic sodium and sulfide-based solid-state electrolytes leads to rapid capacity fading in Na_2MoS_4-Na_3PS_4-based solid-state batteries using sodium metal as the anode.[11] As shown in Figure 3d, the specific capacity

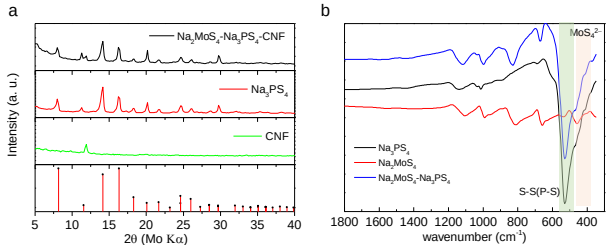

Figure 2 (a) XRD pattern of the Na_2MoS_4-Na_3PS_4-CNF composite cathode. (b) FTIR spectra of the composite cathode compared to those of pure Na_3PS_4 and Na_2MoS_4.

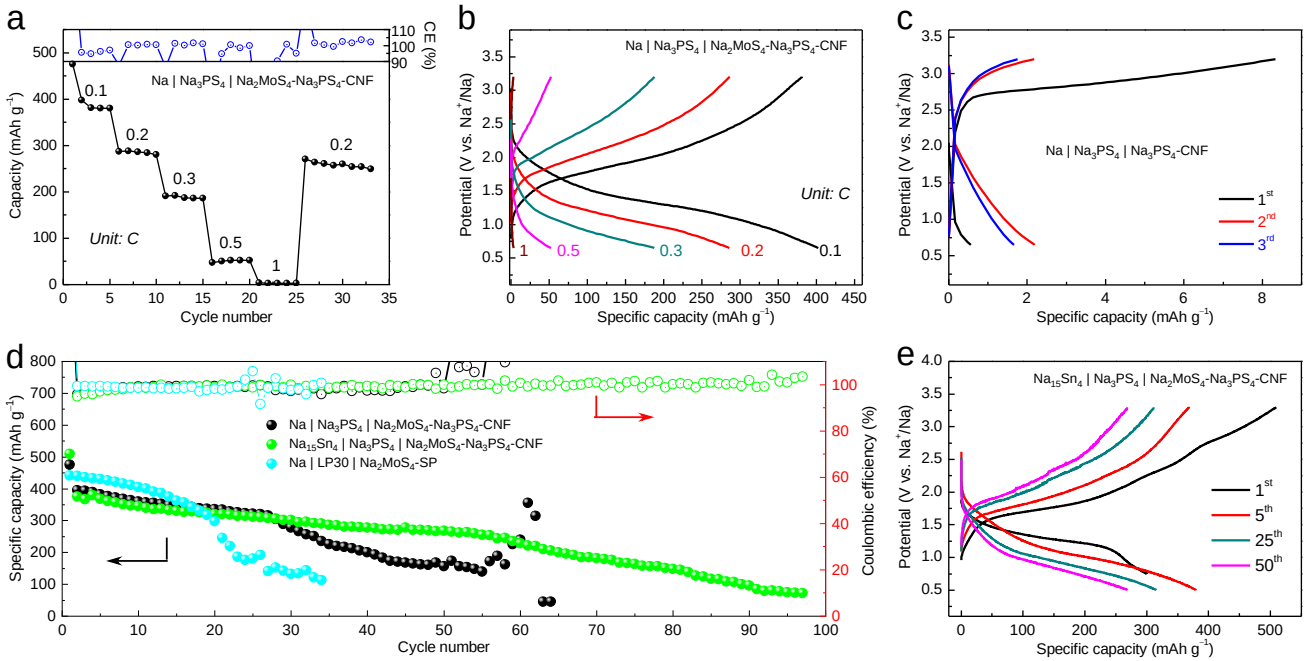

Figure 3 Electrochemical performance of Na_2MoS_4 in Na_3PS_4-based all-solid-state coin cells. (a) Rate capability of the Na | Na_3PS_4 | Na_2MoS_4-Na_3PS_4-CNF solid-state cell (1 C corresponds to 500 mA·g^{-1}). (b) Galvanostatic charge-discharge profiles of the Na | Na_3PS_4 | Na_2MoS_4-Na_3PS_4-CNF cell at various current densities in the voltage range of 0.65–3.2 V (vs. Na^+/Na). (c) Galvanostatic charge–discharge profile of a control cell without Na_2MoS_4: Na | Na_3PS_4 | Na_3PS_4-CNF. (d) Cycling performance of the Na | Na_3PS_4 | Na_2MoS_4-Na_3PS_4-CNF cell at 0.1 C over 50 cycles, compared with the Na | LP30 | Na_2MoS_4-SP cell at 0.2 C, and the $Na_{15}Sn_4$ | Na_3PS_4 | Na_2MoS_4-Na_3PS_4-CNF cell at 0.1 C and 60 °C. (e) Corresponding galvanostatic charge-discharge profiles of the $Na_{15}Sn_4$ | Na_3PS_4 | Na_2MoS_4-Na_3PS_4-CNF solid-state cell at the 1st, 5th, 25th, and 50th cycles at 0.1 C and 60 °C.

declines significantly after only 30 cycles at a current rate of 0.1 C, despite a slight improvement in stability compared to its liquid-electrolyte counterpart. To address this limitation, we employed a $Na_{15}Sn_4$ alloy (Figure S4)—known for its superior chemical and electrochemical compatibility with sulfide solid electrolytes—as the anode material (Figure 3d). As expected, the solid-state battery incorporating the $Na_{15}Sn_4$ alloy anode exhibited excellent cycling stability, maintaining a specific capacity of approximately 268.41 mAh·g^{-1} after 50 cycles (Figure 3e).

Additionally, in coin-type solid-state cells, the low stacking pressure leads to gradually increasing polarization during cycling (Figure 3e). This behavior is attributed to the repeated volume expansion and contraction of the electrodes during sodiation and desodiation, which tends to disrupt the contact between the active materials, electrolyte, and conductive agents, ultimately resulting in performance degradation.[11,37] To address this issue, a polyether ether ketone (PEEK)-based test cell with a pressure-retaining structure was employed for further performance evaluation (Figure S7). The rate performance of the $Na_{15}Sn_4$ | Na_3PS_4 | Na_2MoS_4-Na_3PS_4-CNF solid-state battery using the PEEK device is presented in Figures 4a and 4b. At current rates of 0.1 C, 0.2 C, 0.3 C, 0.5 C, 0.7 C, and 1.0 C, the cell delivers reversible specific capacities of approximately 372, 341, 319, 284, 254, and 214 mAh·g^{-1}, respectively—significantly outperforming the previously constructed Na | Na_3PS_4 | Na_2MoS_4-Na_3PS_4-CNF coin cell. The corresponding Ragone plot further indicates that the specific energy of the Na_2MoS_4-based cell remains relatively stable as the specific power increases, demonstrating its excellent high-power capability (Figure S8). Notably, the optimized $Na_{15}Sn_4$ | Na_3PS_4 | Na_2MoS_4-Na_3PS_4-CNF PEEK cell also demonstrates excellent cycling stability, maintaining nearly 100% capacity retention after over 450 cycles at 0.3 C (Figures 4a and 4c). Compared with most of the previously reported material systems, Na_2MoS_4 delivers a comparable energy density (Figure 4d),[11,33-35] a higher reversible capacity and a longer cycle life (Tables S1 and S2), highlighting its potential for the development of high-energy-density sodium solid-state batteries.

Interfacial properties

Given the excellent electrochemical performance of the

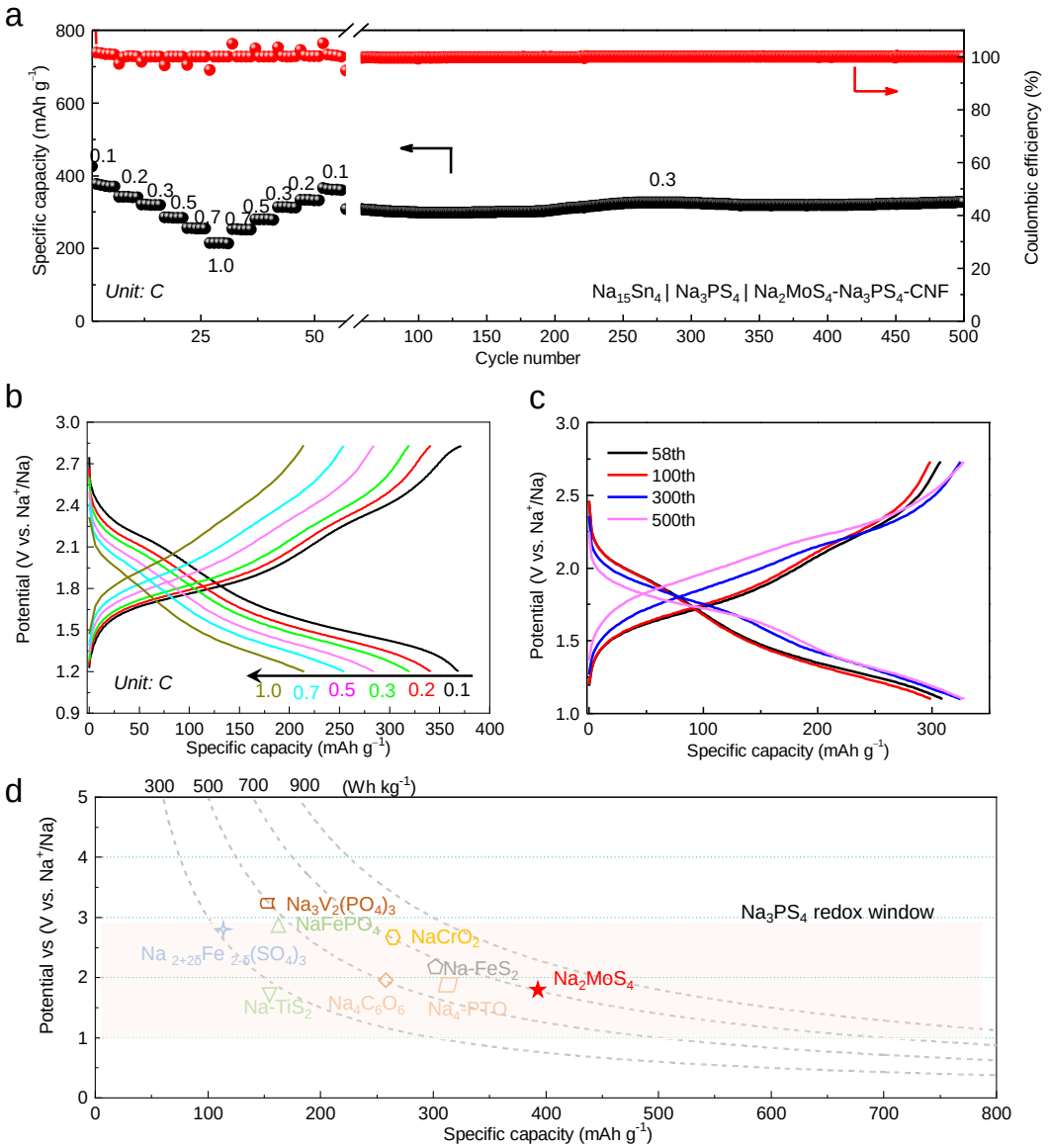

Figure 4 Electrochemical performance of Na_2MoS_4 in Na_3PS_4-based all-solid-state cells with pressure-retaining structure. (a) Rate capability of the $Na_{15}Sn_4$ | Na_3PS_4 | Na_2MoS_4-Na_3PS_4-CNF solid-state cell. (b) Galvanostatic charge-discharge profiles of the $Na_{15}Sn_4$ | Na_3PS_4 | Na_2MoS_4-Na_3PS_4-CNF solid-state cell at various current densities in the voltage range of 1.25–2.83 V (vs. Na^+/Na) at 60 °C. (c) Plot of redox potential versus theoretical specific capacity for reported intercalation-type cathode materials (TiS_2,[10,26-27] $Na_3V_2(PO_4)_3$,[28-29] $NaFePO_4$,[30-31] $Na_{2+2\delta}Fe_{2-\delta}(SO_4)_3$,[32] $NaCrO_2$,[33-34] $Na_4C_6O_6$[35] and Na_4-PTO[11]), Na_2MoS_4 (this work), and a representative conversion-type cathode (FeS_2[36]). Specific capacities are calculated based on the fully sodiated form of each material. Solid squares represent average redox potentials, and open bars denote the corresponding electrochemical windows.

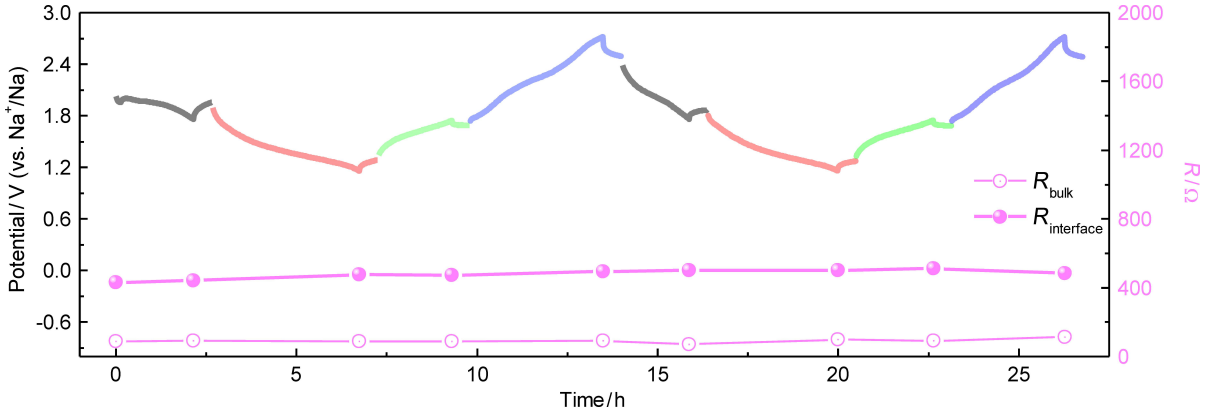

Figure 5 Interfacial properties of the $Na_{15}Sn_4$ | Na_3PS_4 | Na_2MoS_4-Na_3PS_4-CNF all-solid-state cell. Galvanostatic charge-discharge profile during the initial two cycles at 0.1 C and room temperature. Electrochemical impedance spectra recorded at various potentials during cycling.

optimized $Na_{15}Sn_4$ | Na_3PS_4 | Na_2MoS_4-Na_3PS_4-CNF solid-state PEEK cell, we employed *in situ* electrochemical impedance spectroscopy (EIS) to get insights into its interfacial characteristics. Figure S9 presents the EIS spectra recorded at various potentials during the two cycles, along with the equivalent circuit model used for fitting. In this model, R_1, R_2, CPE, and W represent the intrinsic resistance of the solid-state electrolyte (including bulk and grain boundary resistance), the interfacial resistance at the electrode-electrolyte interfaces, the constant-phase element, and the Warburg impedance, respectively. The corresponding fitted results are summarized in Table S3 and Figure 5. Notably, both the intrinsic resistance of the solid-state electrolyte (~90 Ω) and the interfacial resistance (~490 Ω) remain stable during charge-discharge cycling. Further, SEM analysis confirms that the intimate contact among Na_2MoS_4, Na_3PS_4 and CNF is well retained after prolonged cycling (Figure S10), while XPS analysis reveals that the chemical state of the Na_2MoS_4 active material remains largely stable (Figure S11). These findings collectively demonstrate that both the Na_2MoS_4 cathode and $Na_{15}Sn_4$ alloy anode exhibit excellent chemical and electrochemical compatibility with the Na_3PS_4-based solid-state electrolyte, thereby ensuring stable interfacial properties, strong mechanical integrity, and robust cycling performance of the assembled solid-state cell.

Conclusions

In summary, we demonstrate the potential of the inorganic cathode material Na_2MoS_4 for enabling advanced solid-state batteries with high energy density, high power output, and long cycle life. Our findings highlight the critical importance of the cathode's redox electrochemical window, the chemical and electrochemical compatibility among the cathode/anode and solid-state electrolyte, as well as intimate interfacial contact in determining the cycling stability of the solid-state battery. By optimizing these key factors, we successfully realized the efficient application of Na_2MoS_4 in Na_3PS_4-based solid-state battery systems. Specifically, the optimized system delivers exceptional cycling performance, retaining nearly 100% of its capacity over 450 cycles at 0.3 C and achieving an energy density of up to 700 $Wh \cdot kg^{-1}$—surpassing most previously reported solid-state sodium-metal battery systems. The excellent electrochemical performance achieved in this work, along with the deeper insights into electrode-electrolyte interfacial behavior, provides strong impetus for the continued development of high-performance solid-state batteries. Furthermore, these results open new avenues for the application of sulfide-based solid-state devices in next-generation energy storage technologies. Overall, this study represents a significant advance toward the realization of sustainable, safe, and high-efficiency solid-state energy storage systems.

Beyond technical viability, the economic feasibility of Na_2MoS_4 also warrants consideration for future practical deployment. Despite molybdenum being a critical metal with relatively high unit cost, its high theoretical capacity (~500 $mAh \cdot g^{-1}$) substantially reduces the amount of active material required per unit energy. In addition, Na_2MoS_4 can be synthesized via low-temperature, solution-based processes, lowering manufacturing energy consumption and cost relative to conventional oxide cathodes. Its moderate redox potential also aligns well with the electrochemical stability window of sulfide solid electrolytes, avoiding interfacial degradation and eliminating the need for costly protective coatings. Together, these attributes offer a favorable performance-to-cost ratio, supporting the potential of Na_2MoS_4 as a practical and scalable cathode material for solid-state sodium batteries.

Experimental

Materials synthesis

Na_3PS_4 was synthesized via high-energy ball milling. Initially, Na_2S[38] (Sigma-Aldrich, 98% or Nagao, 99.6%) and P_2S_5 (Sigma-Aldrich, 99%) were hand-ground for 1 h. A mixture containing 1 g of Na_2S and P_2S_5, in a molar ratio of 75 : 25, was then loaded into a 45 mL tungsten carbide (WC) milling jar along with two 15 mm WC balls. To maintain an inert atmosphere, the jar was sealed inside an argon-filled glovebox before milling. High-energy ball milling was performed at 25 Hz for 1 h. The resulting powder was transferred into an ampoule, flame-sealed, and annealed in a muffle furnace (Nabertherm, Germany). The furnace temperature was increased from room temperature to 270 °C at a rate of 10 $°C \cdot min^{-1}$ and held at 270 °C for 2 h.

The $Na_{15}Sn_4$ alloy (Figure S4) was prepared following a previously reported method,[35] which provides a redox potential of approximately 0.1 V vs. Na^+/Na. LP30 electrolyte (1 M $LiPF_6$ in EC : DMC, 3 : 7 *V*/*V*) was purchased from Suzhou Fosai New Material Co., Ltd. (China). The synthesis of Na_2MoS_4 followed our previous work.[20] Carbon nanofibers (CNFs) were obtained from Sigma-Aldrich (diameter × length: 100 nm × 20–200 μm), and Super P (SP) carbon black was purchased from TOB New Energy (China).

Materials characterization

Powder X-ray diffraction (XRD) patterns were collected using a STOE StadiP transmission diffractometer (DARMSTADT, Germany) equipped with Mo Kα radiation (λ = 0.71073 Å) to identify the crystalline phases of the synthesized materials. Fourier-Transform Infrared Spectroscopy (FTIR) spectra of pristine powders were recorded using either a Bruker Alpha-P or an Agilent Cary 630 spectrometer, both equipped with a single-reflection ATR module. Electrochemical Impedance Spectroscopy (EIS) measurements of pelletized samples were performed over the frequency range of 100 mHz to 7 MHz using an EC-Lab S-300 impedance analyzer. Carbon-coated aluminum foils were pressed onto both sides of the

pellets to serve as blocking electrodes. Ionic conductivity was measured using an EC-Lab SP-200 impedance analyzer over the same frequency range (100 mHz to 7 MHz). Carbon-coated aluminum foils were applied to both sides of the pellets. The ionic conductivity (σ) was calculated using the equation $\sigma = L/(R \cdot A)$, where L is the pellet thickness, A is the cross-sectional area, and R is the bulk resistance obtained from the high-frequency intercept of the Nyquist plot.

Fabrication and testing of all-solid-state cells

Two types of all-solid-state cells were fabricated: coin cells and polyether-ether-ketone (PEEK) cells. For the coin cell configuration, 130 mg of Na_3PS_4 solid electrolyte was first pressed into a 10 mm diameter pellet under a pressure of 1000 kg for 2 min. Subsequently, 2 mg of composite cathode material was pressed onto one side of the Na_3PS_4 pellet at 4700 kg for 5 min. The Na_2MoS_4-Na_3PS_4-CNF composite cathodes were prepared by manually grinding the components in an agate mortar and pestle for 1 h with weight ratios of x : 70 : (30–x), where x = 0, 10, 15 and 20. Finally, metallic sodium was pressed onto the opposite side of the electrolyte pellet. The assembled solid-state battery was sealed in a CR2016 coin cell casing under 700 kg of pressure. For the PEEK cell, 150 mg of Na_3PS_4 was pressed into a 12 mm diameter pellet under 1000 kg of pressure for 2 min. Next, 100 mg of $Na_{15}Sn_4$ alloy was pressed onto one side of the pellet under 1000 kg of pressure for 2 min. Finally, 3 mg of composite cathode material was pressed onto the other side of the pellet at 5000 kg for 5 min. The PEEK-based cell was enclosed in a metal frame for electrochemical testing. All cells were tested using a Neware battery testing system (China). Tests involving Na_3PS_4 were conducted at 60 °C in a temperature-controlled oven.

Supporting Information

The supporting information for this article is available on the WWW under https://doi.org/10.1002/cjoc.70313.

Acknowledgement

This work was supported by Taiyuan Institute of Technology Scientific Research Initial Funding (2024KL006, 2024LJ002, 2024KJ037), the Scientific and Technological Innovation Programs of Higher Education Institutions in Shanxi (2024L365), Fund Program for the Scientific Activities of Selected Returned Overseas Professionals in Shanxi Province (20240031) and Shanxi Provincial Research Foundation for Basic Research (20210302124219). H. X., J. W., X. L., and X. Z. acknowledge China Scholarship Council for funding. X. L. acknowledges financial support from the Marie Skłodowska-Curie Actions (grant agreement No. 101064286) and the Fonds de la Recherche Scientifique – FNRS (Grant No. 40010559) for his postdoctoral fellowship. Alexandru Vlad acknowledges financial support by INNOVIRIS 2019-RDIR-59B, INNOVIRIS 2024-RDIR-43B, F.R.S.-FNRS through grant No° - F.4552.21 – DEMIST, CF-ARC grant (18/23-093) MICROBAT, FWO and F.R.S.-FNRS under the Excellence of Science (EOS) program - ECOBAT [40007515].

References

[1] Fan, E.; Li, L.; Wang, Z.; Lin, J.; Huang, Y.; Yao, Y.; Chen, R.; Wu, F. Sustainable Recycling Technology for Li-Ion Batteries and Beyond: Challenges and Future Prospects. *Chem. Rev.* **2020**, *120*, 7020–7063.

[2] Nayak, P. K.; Yang, L.; Brehm, W.; Adelhelm, P. From Lithium-Ion to Sodium-Ion Batteries: Advantages, Challenges, and Surprises. *Angew. Chem. Int. Ed.* **2018**, *57*, 102–120.

[3] Lu, Y.; Li, L.; Zhang, Q.; Niu, Z.; Chen, J. Electrolyte and interface engineering for solid-state sodium batteries. *Joule* **2018**, *2*, 1747–1770.

[4] Janek, J.; Zeier, W. G. A solid future for battery development. *Nat. Energy* **2016**, *1*, 16141.

[5] Zhao, C.; Liu, L.; Qi, X.; Lu, Y.; Wu, F.; Zhao, J.; Yu, Y.; Hu, Y. S.; Chen, L. Solid-state sodium batteries. *Adv. Energy Mater.* **2018**, *8*, 1703012.

[6] Xu, P.; Li, X.; Yan, M. Y.; Ni, H.-B.; Huang, H. H.; Lin, X. D.; Liu, X. Y.; Fan, J. M.; Zheng, M.-S.; Yuan, R. M.; Dong, Q. F. A highly reversible sodium metal anode by mitigating electrodeposition overpotential. *J. Mater. Chem. A* **2021**, *9*, 22892–22900.

[7] Wang, Y.; Wang, Z.; Xu, X.; Oh, S. J. A.; Sun, J.; Zheng, F.; Lu, X.; Xu, C.; Yan, B.; Huang, G. Ultra-stable sodium-ion battery enabled by all-solid-state ferroelectric-engineered composite electrolytes. *Nano-Micro Lett.* **2024**, *16*, 254.

[8] Liu, B.; Pu, S. D.; Doerrer, C.; Spencer Jolly, D.; House, R. A.; Melvin, D. L.; Adamson, P.; Grant, P. S.; Gao, X.; Bruce, P. G. The effect of volume change and stack pressure on solid-state battery cathodes. *SusMat* **2023**, *3*, 721–728.

[9] Duchardt, M.; Ruschewitz, U.; Adams, S.; Dehnen, S.; Roling, B. Vacancy-Controlled Na^+ Superion Conduction in $Na_{11}Sn_2PS_{12}$. *Angew. Chem. Int. Ed.* **2018**, *130*, 1365–1369.

[10] Hayashi, A.; Noi, K.; Sakuda, A.; Tatsumisago, M. Superionic glass-ceramic electrolytes for room-temperature rechargeable sodium batteries. *Nat. Commun.* **2012**, *3*, 856.

[11] Hao, F.; Chi, X.; Liang, Y.; Zhang, Y.; Xu, R.; Guo, H.; Terlier, T.; Dong, H.; Zhao, K.; Lou, J.; Yao, Y. Taming Active Material-Solid Electrolyte Interfaces with Organic Cathode for All-Solid-State Batteries. *Joule* **2019**, *3*, 1349–1359.

[12] Tian, Y.; Shi, T.; Richards, W. D.; Li, J.; Kim, J. C.; Bo, S. H.; Ceder, G. Compatibility issues between electrodes and electrolytes in solid-state batteries. *Energy Environ. Sci.* **2017**, *10*, 1150–1166.

[13] Kim, S. W.; Seo, D. H.; Ma, X.; Ceder, G.; Kang, K. Electrode materials for rechargeable sodium-ion batteries: potential alternatives to current lithium-ion batteries. *Adv. Energy Mater.* **2012**, *2*, 710–721.

[14] Pan, H.; Hu, Y. S.; Chen, L. Room-temperature stationary sodium-ion batteries for large-scale electric energy storage. *Energy Environ. Sci.* **2013**, *6*, 2338–2360.

[15] Tang, H.; Deng, Z.; Lin, Z.; Wang, Z.; Chu, I. H.; Chen, C.; Zhu, Z.; Zheng, C.; Ong, S. P. Probing solid–solid interfacial reactions in all-solid-state sodium-ion batteries with first-principles calculations. *Chem. Mater.* **2018**, *30*, 163–173.

[16] Nguyen, H.; Banerjee, A.; Wang, X.; Tan, D.; Wu, E. A.; Doux, J. M.; Stephens, R.; Verbist, G.; Meng, Y. S. Single-step synthesis of highly conductive Na_3PS_4 solid electrolyte for sodium all solid-state batteries. *J. Power Sources* **2019**, *435*, 126623.

[17] Moon, C. K.; Lee, H. J.; Park, K. H.; Kwak, H.; Heo, J. W.; Choi, K.; Yang, H.; Kim, M. S.; Hong, S. T.; Lee, J. H.; Jung, Y. S. Vacancy-Driven Na^+ Superionic Conduction in New Ca-Doped Na_3PS_4 for All-Solid-State Na-Ion Batteries. *ACS Energy Lett.* **2018**, *3*, 2504–2512.

[18] Wan, H.; Mwizerwa, J. P.; Qi, X.; Liu, X.; Xu, X.; Li, H.; Hu, Y. S.; Yao, X. Core-Shell $Fe_{1-x}S@Na_{2.9}PS_{3.95}Se_{0.05}$ Nanorods for Room Temperature All-Solid-State Sodium Batteries with High Energy Density. *ACS Nano* **2018**, *12*, 2809–2817.

[19] Santhosha, A. L.; Medenbach, L.; Palaniselvam, T.; Adelhelm, P. Sodium-Storage Behavior of Exfoliated MoS_2 as an Electrode Material for Solid-State Batteries with Na_3PS_4 as the Solid Electrolyte. *J. Phys. Chem. C* **2020**, *124*, 10298–10305.

[20] Zhu, Q.; Wang, J.; Liu, X.; Ebejer, N.; Rambabu, D.; Vlad, A. Mixed Anionic and Cationic Redox Chemistry in a Tetrathiomolybdate Amorphous Coordination Framework. *Angew. Chem. Int. Ed.* **2020**, *132*, 16722–16729.

[21] Tan, D. H. S.; Wu, E. A.; Nguyen, H.; Chen, Z.; Marple, M. A. T.; Doux, J. M.; Wang, X.; Yang, H.; Banerjee, A.; Meng, Y. S. Elucidating Reversible Electrochemical Redox of Li_6PS_5Cl Solid Electrolyte. *ACS Energy Lett.* **2019**, *4*, 2418–2427.

[22] Lin, X.; Apostol, P.; Xu, H.; Bakuru, V. R.; Guo, X.; Chen, Z.; Rambabu, D.; Pal, S.; Tie, D.; Zhang, Y.; Xie, X.; Kim, S. G.; Li, Y.; Li, Z.; Du, M.; Yan, S.; Zhang, X.; Yuan, R.; Zheng, M.; Gauthy, F.; Finsy, V.; Zou, J.; Gohy, J. F.; Dong, Q.; Vlad, A. Design Principles of Quinone Redox Systems for Advanced Sulfide Solid-State Organic Lithium Metal Batteries. *Adv. Mater.* **2024**, *36*, e2312908.

[23] Chi, X.; Zhang, Y.; Hao, F.; Kmiec, S.; Dong, H.; Xu, R.; Zhao, K.; Ai, Q.; Terlier, T.; Wang, L.; Zhao, L.; Guo, L.; Lou, J.; Xin, H.; Martin, S.; Yao, Y. An electrochemically stable homogeneous glassy electrolyte formed at room temperature for all-solid-state sodium batteries. *Nat. Commun.* **2022**, *13*, 2854.
[24] Ma, L.; Wang, Q.; Islam, S. M.; Liu, Y.; Ma, S.; Kanatzidis, M. G. Highly Selective and Efficient Removal of Heavy Metals by Layered Double Hydroxide Intercalated with the $MoS_4^{(2-)}$ Ion. *J. Am. Chem. Soc.* **2016**, *138*, 2858–66.
[25] Weber, T.; Muijsers, J.; Van Wolput, J.; Verhagen, C.; Niemantsverdriet, J. Basic reaction steps in the sulfidation of crystalline MoO_3 to MoS_2, as studied by X-ray photoelectron and infrared emission spectroscopy. *J. Phys. Chem.* **1996**, *100*, 14144–14150.
[26] Chu, I. H.; Kompella, C. S.; Nguyen, H.; Zhu, Z.; Hy, S.; Deng, Z.; Meng, Y. S.; Ong, S. P. Room-Temperature All-solid-state Rechargeable Sodium-ion Batteries with a Cl-doped Na_3PS_4 Superionic Conductor. *Sci. Rep.* **2016**, *6*, 33733.
[27] Yu, Z.; Shang, S. L.; Seo, J. H.; Wang, D.; Luo, X.; Huang, Q.; Chen, S.; Lu, J.; Li, X.; Liu, Z. K.; Wang, D. Exceptionally High Ionic Conductivity in $Na_{(3)}P_{(0.62)}As_{(0.38)}S_{(4)}$ with Improved Moisture Stability for Solid-State Sodium-Ion Batteries. *Adv. Mater.* **2017**, *29*, 1605561.
[28] Li, Y.; Deng, Z.; Peng, J.; Chen, E.; Yu, Y.; Li, X.; Luo, J.; Huang, Y.; Zhu, J.; Fang, C. A P2-type layered superionic conductor Ga-doped $Na_2Zn_2TeO_6$ for all-solid-state sodium-ion batteries. *Chem. Eur. J.* **2018**, *24*, 1057–1061.
[29] Zhang, Z.; Zhang, Q.; Shi, J.; Chu, Y. S.; Yu, X.; Xu, K.; Ge, M.; Yan, H.; Li, W.; Gu, L. A self-forming composite electrolyte for solid-state sodium battery with ultralong cycle life. *Adv. Energy Mater.* **2017**, *7*, 1601196.
[30] Kim, J. J.; Yoon, K.; Park, I.; Kang, K. Progress in the development of sodium-ion solid electrolytes. *Small Methods* **2017**, *1*, 1700219.
[31] Kim, J. K.; Lim, Y. J.; Kim, H.; Cho, G. B.; Kim, Y. A hybrid solid electrolyte for flexible solid-state sodium batteries. *Energy Environ. Sci.* **2015**, *8*, 3589–3596.
[32] Rao, R. P.; Chen, H.; Wong, L. L.; Adams, S. $Na_{3+x}M_xP_{1-x}S_4$ (M= Ge^{4+}, Ti^{4+}, Sn^{4+}) enables high rate all-solid-state Na-ion batteries $Na_{2+2\delta}Fe_{2-\delta}(SO_4)_3$ | $Na_{3+x}M_xP_{1-x}S_4$ | $Na_2Ti_3O_7$. *J. Mater. Chem. A* **2017**, *5*, 3377–3388.
[33] Banerjee, A.; Park, K. H.; Heo, J. W.; Nam, Y. J.; Moon, C. K.; Oh, S. M.; Hong, S. T.; Jung, Y. S. Na_3SbS_4: a solution processable sodium superionic conductor for all-solid-state sodium-ion batteries. *Angew. Chem. Int. Ed.* **2016**, *128*, 9786–9790.
[34] Duchêne, L.; Kühnel, R. S.; Stilp, E.; Reyes, E. C.; Remhof, A.; Hagemann, H.; Battaglia, C. A stable 3 V all-solid-state sodium-ion battery based on a closo-borate electrolyte. *Energy Environ. Sci.* **2017**, *10*, 2609–2615.
[35] Chi, X.; Liang, Y.; Hao, F.; Zhang, Y.; Whiteley, J.; Dong, H.; Hu, P.; Lee, S.; Yao, Y. Tailored organic electrode material compatible with sulfide electrolyte for stable all-solid-state sodium batteries. *Angew. Chem. Int. Ed.* **2018**, *57*, 2630–2634.
[36] Wan, H.; Mwizerwa, J. P.; Qi, X.; Xu, X.; Li, H.; Zhang, Q.; Cai, L.; Hu, Y. S.; Yao, X. Nanoscaled Na_3PS_4 solid electrolyte for all-solid-state FeS_2/Na batteries with ultrahigh initial coulombic efficiency of 95% and excellent cyclic performances. *ACS Appl. Mater. Interfaces* **2018**, *10*, 12300–12304.
[37] Schwietert, T. K.; Arszelewska, V. A.; Wang, C.; Yu, C.; Vasileiadis, A.; de Klerk, N. J. J.; Hageman, J.; Hupfer, T.; Kerkamm, I.; Xu, Y.; van der Maas, E.; Kelder, E. M.; Ganapathy, S.; Wagemaker, M. Clarifying the relationship between redox activity and electrochemical stability in solid electrolytes. *Nat. Mater.* **2020**, *19*, 428–435.
[38] Zhang, W.; Duan, Y.; Chi, X.; Tan, W.; Weng, W.; Zhong, S. Extraction of Mn and Sr from electrolytic zinc slime using SO_2-containing flue gas as reductant. *Sep. Purif. Technol.* **2025**, *366*, 132787.

Manuscript received: July 22, 2025
Manuscript revised: September 10, 2025
Manuscript accepted: September 15, 2025
Version of record online: October 11, 2025

The Authors

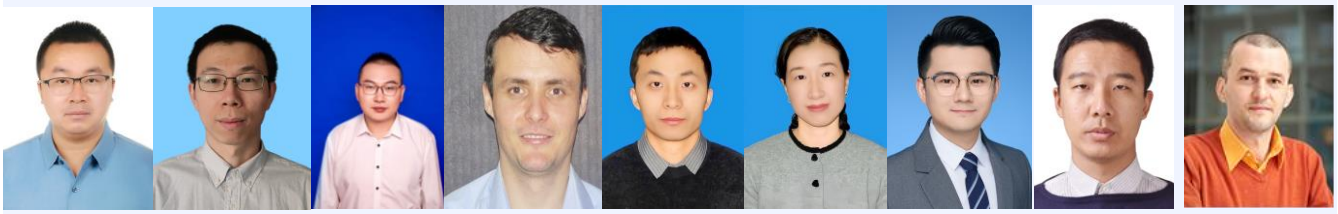

Left to Right: Hewei Xu, Xiaodong Lin, Hong Chang, Petru Apostol, Jiande Wang, Xuelian Liu, Xiaozhe Zhang, Da Tie, Alexandru Vlad

